Investigation of the reaction ^{74}Ge(p,γ)^{75}As using the in-beam method to improve reaction network predictions for p nuclei

A. Sauerwein,* J. Endres, L. Netterdon, and A. Zilges

Institut für Kernphysik, Universität zu Köln, Zülpicher Straße 77, 50937 Köln, Germany

V. Foteinou, G. Provatas, T. Konstantinopoulos, M. Axiotis, S. F. Ashley, and S. Harissopulos

Tandem Accelerator Laboratory, Institute of Nuclear Physics,
NCSR "Demokritos", 153.10 Aghia Paraskevi, Athens, Greece

T. Rauscher

Department of Physics, University of Basel, Klingelbergstraße 82, 4056 Basel, Switzerland
(Dated: September 18, 2012)

Background: Astrophysical models studying the origin of the neutron-deficient p nuclides require the knowledge of proton capture cross sections at low energy. The production site of the p nuclei is still under discussion but a firm basis of nuclear reaction rates is required to address the astrophysical uncertainties. Data at astrophysically relevant interaction energies are scarce. Problems with the prediction of charged particle capture cross sections at low energy were found in the comparisons between previous data and calculations in the Hauser-Feshbach statistical model of compound reactions.

Purpose: A measurement of ^{74}Ge(p,γ)^{75}As at low proton energies, inside the astrophysically relevant energy region, is important in several respects. The reaction is directly important as it is a bottleneck in the reaction flow which produces the lightest p nucleus ^{74}Se. It is also an important addition to the data set required to test reaction-rate predictions and to allow an improvement in the global p+nucleus optical potential required in such calculations.

Method: An in-beam experiment was performed, making it possible to measure in the range $2.1 \leq E_p \leq 3.7$ MeV, which is for the most part inside the astrophysically relevant energy window. Angular distributions of the γ-ray transitions were measured with high-purity germanium detectors at eight angles relative to the beam axis. In addition to the total cross sections, partial cross sections for the direct population of twelve levels were determined.

Results: The resulting cross sections were compared to Hauser-Feshbach calculations using the code SMARAGD. Only a constant renormalization factor of the calculated proton widths allowed a good reproduction of both total and partial cross sections. The accuracy of the calculation made it possible to check the spin assignment of some states in ^{75}As. In the case of the 1075 keV state, a double state with spins and parities of $3/2^-$ and $5/2^-$ is needed to explain the experimental partial cross sections. A change in parity from $5/2^+$ to $5/2^-$ is required for the state at 401 keV. Furthermore, in the case of ^{74}Ge, studying the combination of total and partial cross sections made it possible to test the γ width, which is essential in the calculation of the astrophysical ^{74}As(n,γ)^{75}As rate.

Conclusions: Between data and statistical model prediction a factor of about two was found. Nevertheless, the improved astrophysical reaction rate of ^{74}Ge(p,γ) (and its reverse reaction) is only 28% larger than the previous standard rate. The prediction of the ^{74}As(n,γ)^{75}As rate (and its reverse) was confirmed, the newly calculated rate differs only by a few percent from the previous prediction. The in-beam method with high efficiency detectors proved to be a powerful tool for studies in nuclear astrophysics and nuclear structure.

I. INTRODUCTION

About 35 proton-rich nuclei [1–3], the so-called p nuclei, cannot be synthesized by neutron capture reactions via the s and r process [4–8]. The actual astrophysical environment for the production of the p nuclei is still under discussion. The long-time favored site, explosive burning in the O/Ne shell of massive stars before and during a supernova explosion, was found to underproduce significantly the light p nuclei with $A < 100$ [3, 9–12]. An alternative would be that not just a single process is responsible for all p nuclei but that different processes in a number of astrophysical sites produce certain ranges of p nuclei

(see [13] and references therein). In the search for the p-nucleus production mechanism a number of processes were suggested, such as the γ process in massive stars [9, 12], the rp process [14, 15], the pn process [16], and the νp process [17]. The p nuclei ^{180}Ta and ^{138}La may additionally need contributions from a ν process [18]. A recent study [19] found that light p nuclei are produced in sufficient amounts to explain the abundances in the solar system by a combination of proton capture reactions and photodisintegrations in the thermonuclear explosion of a white dwarf (type Ia supernova), although earlier simulations did not predict such a production [20–22].

In total, these processes include several thousands of reactions on thousands of mainly unstable nuclei. This indicates already that it is not possible to measure all these reaction rates in the laboratory. Therefore, with very few exceptions, the astrophysical reaction rates are
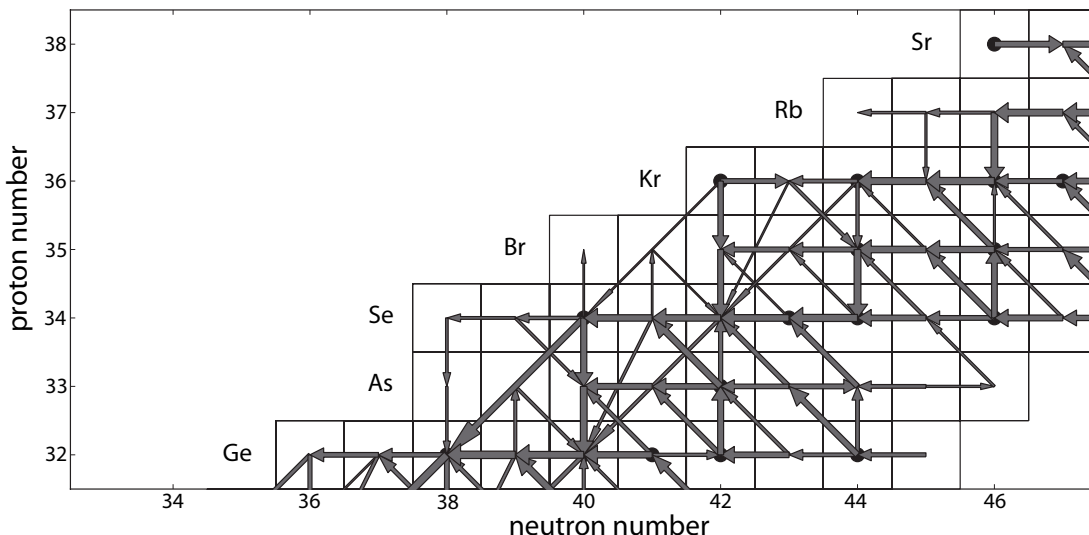
* sauerwein@ikp.uni-koeln.de

FIG. 1. Reaction flow f in the γ process in the vicinity of the p nucleus ^{74}Se. Depicted are time-integrated fluxes from the layer of a 25 $M_\odot$ star which effectively produces ^{74}Se when the shockfront of a core-collapse supernova explosion is passing through. Arrow thicknesses give the magnitude of the flow on a logarithmic scale.

calculated by means of the statistical Hauser-Feshbach model [23]. Nuclear physics input, such as ground state (g.s.) properties, level densities, γ-ray strength functions, and optical model potentials are needed for these calculations. This input can be determined, tested, and improved by laboratory measurements to finally obtain robust and reliable model predictions for these parameters.

It was pointed out [24, 25] that certain reactions are of particular importance in the γ-process reaction network, because a change in their reaction rate has a direct impact on the calculated p nuclei abundance. One of these particular important reactions is the proton capture reaction on ^{74}Ge. It is the first reaction in the sequence ^{74}Ge(p,γ)^{75}As(p,n)^{75}Se(γ,n)^{74}Se, a main production route to the p nucleus ^{74}Se. A strong reaction flow is found to proceed through this sequence as illustrated in Fig. 1, showing the results of our γ-process calculation in a 25 M$_\odot$ star using similar conditions as in Refs. [9, 24] but employing updated reaction rates.

The reaction ^{74}Ge(p,γ)^{75}As was investigated using the in-beam technique, where the γ decay after proton capture is analyzed with high-resolution high-purity germanium detectors [26, 27]. This method makes it possible to investigate besides the total cross section the partial cross section for the direct population of several states in ^{75}As. This is an advantage compared to the widely used activation technique [28–33], which was not applicable anyway since the reaction product ^{75}As is stable.

The method followed here was already demonstrated by Galanopoulos *et al.* [27] of being very powerful to determine very small cross sections, down to 1 μb for astrophysics applications. This makes possible an investigation of the ^{74}Ge(p,γ) reaction between $E_p = 2.1$ MeV and $E_p = 3.7$ MeV.

II. ASTROPHYSICALLY RELEVANT ENERGY WINDOW AND SENSITIVITIES OF ^{74}Ge(p, γ)^{75}As

It is very important to measure close to or inside the astrophysically relevant energy range to ensure that dependencies on nuclear properties are similar to those appearing in the stellar rates because these sensitivities strongly vary with energy. The sensitivities of the astrophysical reaction rate of ^{74}Ge(p,γ)^{75}As to a change in the averaged γ, neutron, proton, and α widths used in the rate and cross-section models are shown in Fig. 2. Here, the averaged widths were varied separately by a factor of two. A sensitivity $s = 1$ indicates that the rate is changed by the same factor as the width, while $s = 0$ signifies that the width variation has no influence on the predicted rate. Details on the calculation of the sensitivity factor s can be found in [34, 35].

As can be seen in Fig. 2, the rate prediction is almost exclusively sensitive to the proton width below about 4 GK, with the relevant stellar plasma temperature T for this reaction in the γ process being close to 3 GK. This rate sensitivity is related to the sensitivity of the reaction cross sections for ^{74}Ge nuclei being in the g.s. and thermally excited states in the energy range mostly contributing to the reaction rate integral $\mathcal{I}$, appearing in the calculation of the stellar rate,

$$\mathcal{I} = \int_0^\infty \sigma^{\text{eff}}(E)\,\Phi(E,T)\,dE \quad , \quad (1)$$

where $\Phi(E,T)$ is the Maxwell-Boltzmann energy distribution of the projectiles and $\sigma^{\text{eff}}(E)$ is the *effective* cross section summing over all energetically possible transitions to states μ, ν in the initial and final nucleus, respectively, [34]

$$\sigma^{\mathrm{eff}} = \sum_\mu \sum_\nu \frac{2J_\mu + 1}{2J_0 + 1} \frac{E - E_\mu}{E} \sigma^{\mu \to \nu}(E - E_\mu) \quad . \quad (2)$$

Following Ref. [36], the above equation implicitly assumes that cross sections $\sigma^{\mu \to \nu}$ at zero or negative energies $E - E_\mu$ are zero. In general, the effective cross section includes more transitions than the laboratory cross section $\sigma^{\mathrm{lab}} = \sum_\nu \sigma^{0 \to \nu}$. However, it depends on the reaction and plasma temperature whether the additional transitions are contributing significantly. Their relative contribution to the stellar rate is given by $1 - X$, where X is the g.s. contribution to the stellar rate [37]

$$X(T) = \frac{\int_0^\infty \sigma^{\mathrm{lab}}(E)\,\Phi(E, T)\,dE}{\int_0^\infty \sigma^{\mathrm{eff}}(E)\,\Phi(E, T)\,dE} \quad . \quad (3)$$

For ^{74}Ge(p,γ)^{75}As at $T = 3$ GK, the integral $\mathcal{I}$ is dominated by contributions from energies $1.5 \leq E \leq 3.1$ MeV [38]. Therefore, our measurement covers a significant fraction of the relevant energy range. However, the g.s. contribution to the stellar rate at 3 GK is $X = 0.66$; that is, only 2/3 of the stellar rate is obtained by integrating the laboratory cross section. Nevertheless, the sensitivity of σ^{lab} in the lower part of the measured energy range, shown in Fig. 3, is similar to the one of the astrophysical reaction rate; that is, there is a dominant sensitivity to variations in the proton width. The calculated proton width depends on nuclear masses (determining the relative energies in all reaction channels), the level schemes, and the proton+nucleus optical potential [34, 35]. Masses and level schemes for nuclei close to the valley of stability are known with sufficient accuracy. Hence, they are no major source of uncertainty in the calculation of the proton width. Therefore, this measurement of the ^{74}Ge(p,γ) reaction is well suited to test the proton optical potential used in the prediction of the rate and to improve the astrophysical reaction rate at γ-process temperatures.

The experimental details of the measurement are presented in Sec. III. After introducing the in-beam technique, the data analysis is presented in Sec. IV. The deduced total and partial cross sections are compared to theoretical predictions from Hauser-Feshbach statistical model calculations in Sec. V, where also final conclusions regarding the astrophysical reaction rate are given.

III. EXPERIMENT

The reaction ^{74}Ge(p,γ)^{75}As (Q value: (6898.94 $\pm$ 0.95) keV [39]) was measured at seven energies partly inside the Gamow window. The proton energies were varied between $2.1 \leq E_p \leq 3.7$ MeV.
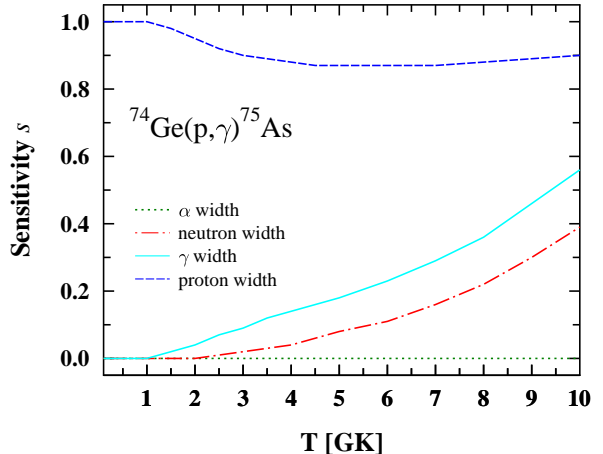

FIG. 2. (Color online) Sensitivities s of the astrophysical reaction rate for ^{74}Ge(p,γ)^{75}As as a function of stellar plasma temperature T when varying neutron, proton, α, and γ widths separately by a factor of two. The relevant temperature in the γ process is close to $T = 3$ GK.

FIG. 3. (Color online) Sensitivities s of the ^{74}Ge(p,γ)^{75}As cross section when varying neutron, proton, α, and γ widths separately by a factor of two. The astrophysical energy window for a temperature of $T = 3$ GK is marked by the shaded area.

A. Preparation and characterization of targets

Germanium, with an enrichment in ^{74}Ge of 97.8 %, was evaporated in vacuum onto a 80 $\frac{\mathrm{mg}}{\mathrm{cm}^2}$-thick gold foil. This backing was thick enough to stop the proton beam completely to ensure a reliable charge collection. The germanium target was characterized by Rutherford back scattering (RBS). The areal density of the target is (301 $\pm$ 12) $\frac{\mu\mathrm{g}}{\mathrm{cm}^2}$, which corresponds to an average en-

ergy loss of about 22 keV and 14 keV at $E_p = 2.1$ MeV and $E_p = 3.7$ MeV, respectively. The energy losses were calculated using the SRIM code [40]. To study the homogeneity of the target thickness, the areal density was determined at many positions of the target area. All measurements yielded the same thickness within the statistical uncertainties. A second RBS measurement after the experiment excluded losses of target material and deterioration effects.

B. Experimental setup

The measurements were carried out at the 5.5 MV T11 Van de Graaff tandem accelerator of the Institute of Nuclear Physics of the National Center for Scientific Research (NCSR) "Demokritos". The accelerator was calibrated by means of the 992–keV resonance of the ^{27}Al(p,γ)^{28}Si reaction. The air-cooled germanium target was bombarded for several hours with protons at beam currents of about 250 nA. The beam, which had a diameter of 4 mm, impinges perpendicular on the target. The beam current was determined by the charge deposited in the backing with a current integrator with an uncertainty of less than 4 %. A negatively charged diaphragm ($U = -400$V) suppresses secondary electrons at the entrance of the target chamber.

The proton capture reactions were identified by detecting the prompt γ decays of the reaction products with four high-purity germanium (HPGe detectors). Three detectors have a relative detection efficiency of 100%, whereas the fourth detector has a relative efficiency of 80% compared to a 7.62×7.62–cm cylindrical NaI detector at $E_\gamma = 1.33$ MeV. The detectors were mounted as close as possible around the target chamber at a distance of 16 cm on a turnable table under fixed angles of $0°$, $90°$, $190°$, and $305°$ relative to the beam axis. After each measurement, this table was rotated by an angle of $15°$ and the target was bombarded with the same energy to measure at four further angles of $15°$, $105°$, $205°$, and $320°$ relative to the beam axis. The proton beam impinged also on a blank gold backing for each energy and each table position, to investigate possible yield contributions from reactions occurring in the backing material. Singles spectra were taken using the same target in all measurements. A typical spectrum for a proton energy of 3.3 MeV is shown in Fig. 4(a)-4(d). This spectrum was recorded with a detector at $0°$ relative to the beam axis. Because of the large distance between detector and target summing effects of the γ rays are negligible ($< 1\%$), which was checked with a GEANT4 simulation [41].
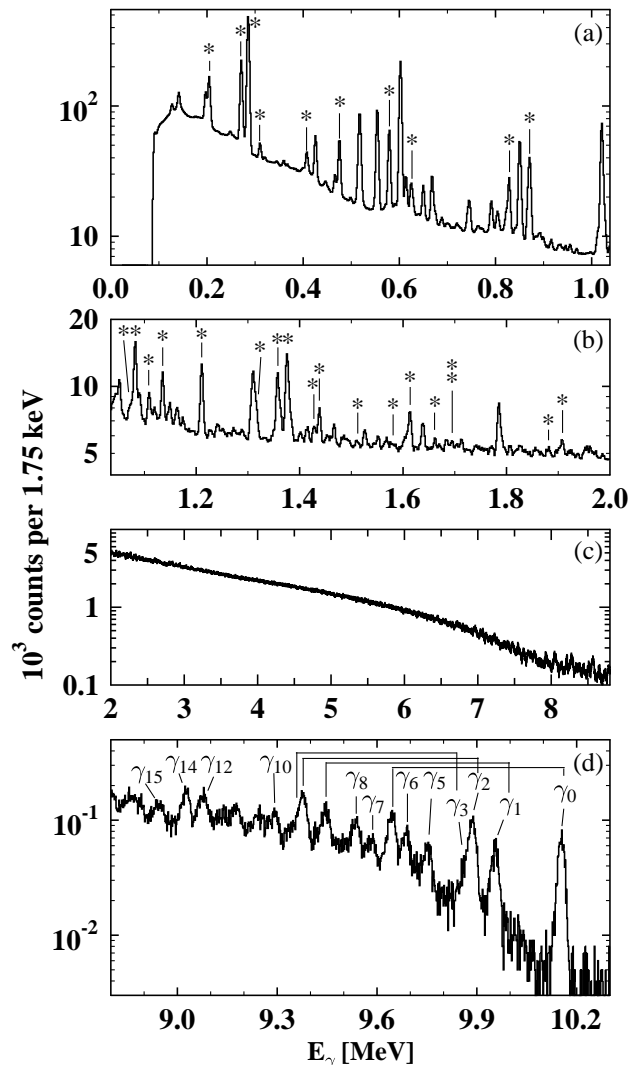

FIG. 4. Typical spectrum while bombarding ^{74}Ge with 3.3–MeV protons. This spectrum was recorded at $0°$ relative to the beam axis. All transitions to the g.s. of the reaction product ^{75}As are marked with an asterisk. Transitions from the so-called entry state to the g.s. or one of the excited states are marked with γ_X. In particular, the transition to the g.s. is denoted by γ_0, whereas the transition to the first excited state is denoted by γ_1 and so on. For some of these transitions the single escape peak is marked as well.

IV. DATA ANALYSIS

A. Production of the compound nucleus

To understand the data analysis of this in-beam experiment, it is useful to discuss the capture mechanism which leads to the formation of a compound nucleus. The target is bombarded with protons of energy E_p to form a highly excited compound nucleus at the energy $E_X = S_p + E_{c.m.}$, where S_p is the proton separation energy in the compound nucleus and $E_{c.m.}$ is the center-of-mass energy.
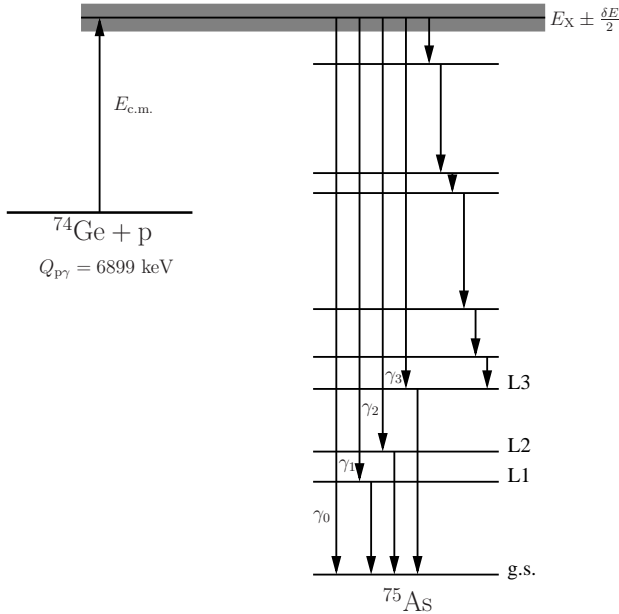
FIG. 5. Schematic illustration of the reaction mechanism and decay. The target nucleus is bombarded with protons to produce a compound nucleus in an excited state with energy E_X. $E_{c.m.}$ denotes the center-of-mass energy of the system. An entry state is de-excited either via a direct γ ray to the ground or to excited states (denoted as γ_0, γ_1, ...). Each observed γ ray is actually a sum of the γ rays emitted by all entry states around E_X.
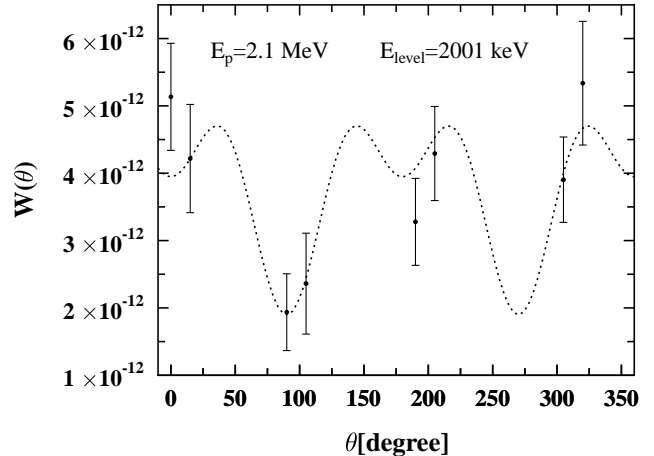

FIG. 6. Angular distribution for the γ-ray transition from the level with energy $E_{\text{level}} = 2001$ keV to the g.s. for an incident energy of $E_p = 2.1$ MeV. The dotted curve corresponds to the Legendre polynomial fitted to the data points.

The proton separation energy is equal to the reaction Q value of proton capture. The reaction mechanism and the decays are illustrated in Fig. 5. In practice, there is a large number of resonances which cannot be resolved within the energy uncertainty δE when the nuclear level density is sufficiently high. This is fulfilled in ^{75}As at basically all projectile energies. The energy uncertainty δE depends on the spread of the initial beam energy and the energy loss in the target. In this experiment the energy uncertainty is about ± 7 keV for all energies. Therefore, not only one discrete entry state is excited but a large number of states in a small energy interval. The measurement includes the formation and decay of all these entry states simultaneously.

The g.s. can be populated by a single γ-ray transition directly from the entry energy as well as by cascades of γ rays populating and depopulating various excited levels, as sketched in Fig. 5. The former transition is the so-called γ_0 transition with an energy $E(\gamma_0) \approx E_X$. The direct feeding of the first excited level L_1 or of the second excited level L_2 results in the γ_1 transition or in the γ_2 transition, respectively, and so on. For each entry state the total γ width Γ_γ is the sum of all partial widths Γ_0, Γ_1, ..., to the final states, $\Gamma_\gamma = \Gamma_0 + \Gamma_1 + \ldots$. The observed strengths and widths of the γ-ray transitions to discrete states, in turn, are actually the sum of the discrete transitions from each entry state around E_X which cannot be resolved individually.

The statistical Hauser-Feshbach model of compound reactions – used in the prediction of astrophysical reaction rates for this reaction – uses the fact that the compound resonances cannot be resolved when encountering many states with widths larger than their spacing. Instead of considering the sums of hundreds of resonances with tiny energy differences, it is equivalent [23, 34] to calculate the formation and decay widths by assuming that states with all spins and parities are present at each E_X, with widths representing the *average* of the widths of all overlapping resonances within δE. These are the averaged widths used in the sensitivity study shown in Sec. I and also used in the theoretical discussion of the experimental results in Sec. V.

B. Determination of the total cross sections

To determine the total cross section of a capture reaction leading to the formation of a compound nucleus, the absolute number of produced compound nuclei N_{comp} has to be determined:

$$N_{\text{comp}} = \sigma \cdot N_p \cdot m_T . \tag{4}$$

The absolute number of projectiles N_p can be calculated from the accumulated charge and the areal particle density in $\frac{1}{\text{cm}^2}$ is denoted as m_T. The absolute number of produced compound nuclei was obtained for each beam energy by measuring the angular distributions of all γ rays to the g.s. of the produced compound nucleus. This is done by measuring the intensities $Y(E_\gamma)$ of all

the relevant γ-ray transitions at eight angles θ relative to the beam axis. First, these intensities are normalized to the corresponding number of projectiles and the absolute full-energy efficiency of the respective detector $\epsilon(E_\gamma)$. The resulting normalized intensities are further corrected by the ratio between live and real time $\tau = \frac{t_{\text{LIVE}}}{t_{\text{REAL}}}$ of the data acquisition system. For a certain detector, which is mounted at an angle θ_A relative to the beam axis, and a g.s. transition with energy E_γ, this normalized intensity is named

$$W(\theta_A) = \frac{Y(E_\gamma)}{\epsilon(E_\gamma)\ \tau\ N_p} \quad . \tag{5}$$

Hence, at each beam energy an angular distribution for each γ-ray transition is obtained by fitting by a sum of Legendre polynomials to the eight experimental $W(\theta_X)$ values:

$$W(\theta) = A_0^i \left(1 + \sum_k \alpha_k P_k\left(cos\theta\right)\right) \quad (k=2,4,..) \quad . \tag{6}$$

The coefficients α_k, which are adjusted to reproduce the experimental angular distributions, are energy dependent. The maximum value of index k depends on the multipolarity of the γ-ray transition in consideration. The scaling factor A_0^i is proportional to the number of produced compound nuclei, which are deexcited via a cascade involving the g.s. transition i. As an example, Fig. 6 shows the angular distribution for the γ-ray transition from the 2001–keV level to the g.s. for an incident energy of $E_p = 2.1$ MeV. For every γ-ray transition i to the g.s. of the produced compound nucleus, an A_0^i coefficient is obtained. The total number of coefficients is N. The absolute number of produced compound nuclei per projectile is equal to the number of emitted γ rays directly to the g.s. per projectile into the whole solid angle and can be derived from

$$\frac{N_{\text{comp}}}{N_p} = \sum_{i=1}^{N} A_0^i \quad . \tag{7}$$

The total cross section is then given by the expression:

$$\sigma = \frac{\sum_{i=1}^{N} A_0^i}{m_T} \quad . \tag{8}$$

As can be seen in Eqs. (7) and (8), only the scaling factor A_0^i contributes to the total cross section. The shape of the angular distribution does not contribute. This is attributable to the fact that an integral over the whole solid angle of a sum of Legendre polynominals vanishes. In this experiment, 35 g.s. transitions were observed for each angle. The corresponding levels are depicted in Fig. 7. In total, 1960 peaks in the spectra had to be analyzed to obtain the total cross section of this reaction for seven energies.
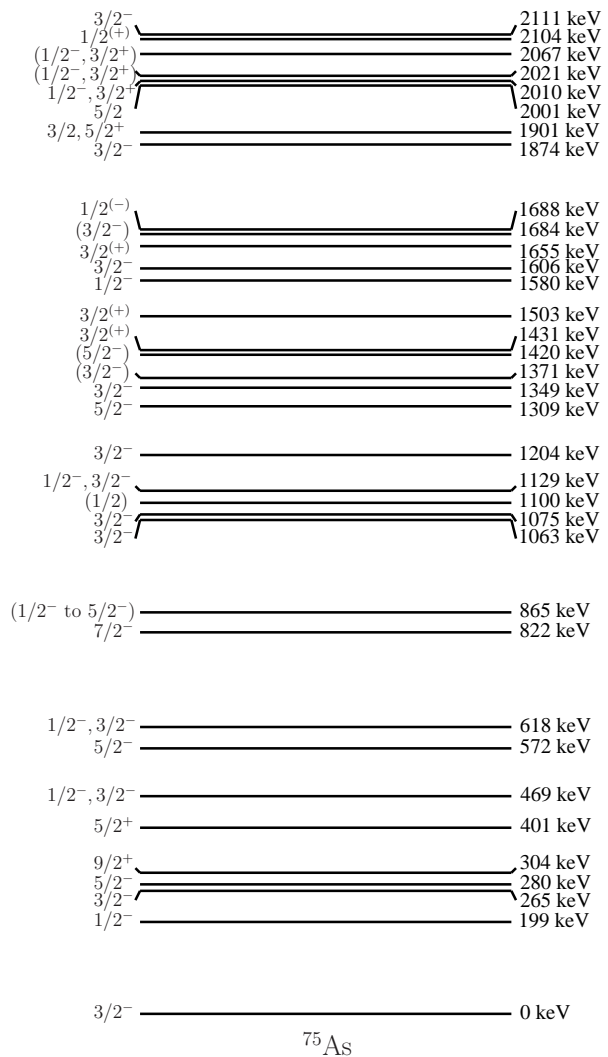

FIG. 7. Partial level scheme of ^{75}As showing all those levels from which transitions to the g.s. were observed in this experiment. All these transitions were taken into account in the determination of the total cross section. The excitation energies E_X, as well as the spins and parities shown were adopted from the compilation of Ref. [42].

C.   Determination of the partial cross sections

It has to be emphasized that owing to the high efficiency of the setup, several γ-ray transitions, which depopulate the entry state, were observed. For each of these γ-ray transitions j the angular distribution were determined with the procedure described in Sec. IV B. From the coefficients A_0^j the partial cross sections were determined by:

$$\sigma^j = \frac{A_0^j}{m_T} \quad . \tag{9}$$

In total, 12 partial cross sections were deduced in this way.

D. Determination of the detector efficiencies

For the calculation of the total and partial cross sections the absolute full-energy efficiencies of the four detectors, at two angles each, have to be known. Because the efficiencies were needed up to energies of about 12 MeV, besides calibration sources the ^{27}Al(p,γ) reaction was used for the efficiency calibration. For this purpose, the resonance at $E_p = 992$ keV was used. For the ^{27}Al(p,γ) reaction relative efficiency curves were first determined using the branchings reported in Ref. [43]. These branchings agree with those reported in Ref. [44] within 5 %. The obtained relative efficiency curves from this reaction were matched to the absolute efficiencies gained with calibration sources.

V. RESULTS AND DISCUSSION

A. Total cross sections

1. Experimental results

The experimental total cross sections are given in Table I and shown in Fig. 8. The experimental values are not corrected for electron screening [45, 46]. An electron screening correction, similar to the one used in Ref. [47, 48], would lead to an decreasing of the cross section of about 5 % and 2 % for the lowest and highest energies measured in this experiment, respectively. The energy E_p of the protons was obtained by correcting the adjusted primary energy E_0 of the proton beam with the average energy loss ΔE inside the target material

$$E_p = \frac{E_0 + (E_0 - \Delta E)}{2} \quad . \tag{10}$$

This energy determination, which is appropriate if the energy loss and the cross section change only slightly over the target thickness, is independent of a specific cross section prediction. In this case, the uncertainties of the cross sections are larger than the changes in the cross section over the target thickness. The widths of the energies are determined by the uncertainty of the beam energy of the accelerator and the straggling in the target. They were added according to Gaussian error propagation. The energy uncertainty of the tandem accelerator at Demokritos was determined by scanning the resonance in ^{27}Al(p,γ)^{28}Si at 992 keV. An energy uncertainty of ± 3.8 keV was found. The energy loss of the protons in the target itself is obtained by a GEANT4 [41] simulation and results in $(14 - 22)$ keV, which agrees with the values obtained with SRIM (compare Sec. III A). The distribution of the proton beam after traveling through the target material is described by this simulation. The maximum of this distribution is $E_0 - \Delta E$ and the half width of this distribution at $1/e$ of the maximum is the energy straggling in the target which was about 6 keV for all
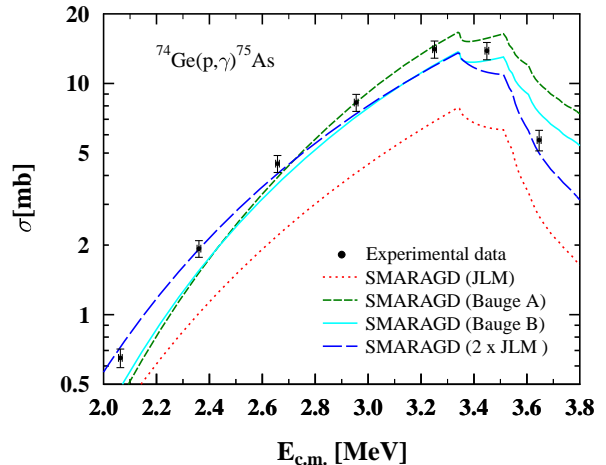

FIG. 8. (Color online) Total cross sections for the reaction ^{74}Ge(p,γ)^{75}As as a function of center-of-mass energy. The total experimental cross sections are compared to predictions with the SMARAGD code [49] using different averaged proton widths from [51] with low-energy modifications of [52] (JLM), [59] (Bauge A), and [60] (Bauge B). Furthermore, the experimental values are compared to predictions using the doubled value of the proton widths from (JLM), denoted as $(2 \times$ JLM) in the figure.

energies. Note that Table I gives center-of-mass energies to facilitate comparison with theoretical calculations.

2. Implications for astrophysical proton capture on ^{74}Ge

In Fig. 8, the experimental values are compared to statistical model calculations performed with the code SMARAGD [49], which includes more current level schemes [42] and an improved calculation method compared to the NON-SMOKER code used in Ref. [50]. As discussed in Sec. I and shown in Fig. 3, the capture cross sections below the (p,n) threshold are mainly sensitive to the proton width and the only uncertainty in this width stems from the optical proton+nucleus potential applied in the calculation. The potential from Ref. [51] with low-energy modifications introduced in Ref. [52] is used as a standard potential. It is named 'JLM' in Fig. 8. The JLM potential yields an underestimation of the measured data by almost a factor of two, while the overall energy dependence is described well, also at the opening of the (p,n) channel where width fluctuation corrections have to be applied.

Exploratory calculations with different optical potentials and input to the potentials were performed. The microscopic JLM potential requires a nuclear matter density as input. The standard calculation shown here makes use of the nuclear matter density HFB-02 [53]. Using density distributions from the droplet model from HFB-14 [54]

TABLE I. Summary of the experimental ^{74}Ge(p,γ) cross sections listed for each center-of-mass energy $E_{\text{c.m.}}$.

$E_{\text{c.m.}}$ [keV]	2063 ± 7	2360 ± 7	2657 ± 7	2955 ± 7	3251 ± 7	3449 ± 7	3646 ± 8
σ [mb]	0.65 ± 0.06	1.93 ± 0.16	4.5 ± 0.4	8.3 ± 0.7	14.1 ± 1.2	13.9 ± 1.2	5.7 ± 0.6

or from Ref. [55] slightly changed the energy dependence but did not affect the magnitude of the cross section significantly. Recently, a modification of the imaginary part of the JLM potential was suggested to explain the energy dependence of low-energy (p,γ) data [34, 56–58]. Again, the impact here is negligible and it cannot account for the discrepancy of a factor of two. A comparison of the ^{74}Ge(p,γ)^{75}As data to results obtained with two additional optical potentials is shown in Fig. 8 as well. Both are a reparametrization of the potential by Ref. [51] using modern scattering data, with one (case A, [59]) being directly based on Ref. [51] and the other (case B, [60]) being a Lane-consistant version. These potentials are named 'Bauge A' and 'Bauge B' in Fig. 8. Unfortunately, both do not include low-energy modifications as suggested by Ref. [52]. As seen in Fig. 8, both reparametrizations give a better estimation of the absolute magnitude of the cross sections in the measured energy region but they exhibit a different energy dependence. A good reproduction of the energy dependence, however, is crucial for the prediction of the astrophysical reaction rate, as relevant contributions to the reaction rate integral defined in Eq. (1) also come from energies lower than the measured ones.

Because the standard JLM potential accounts for the correct energy dependence of the cross sections, in the following we use the proton widths of this potential but multiply them by a factor of two. The resulting cross sections are also shown in Fig. 8. We obtain ratios between the SMARAGD predictions using the increased proton widths and the experimental (p,γ) cross sections close to unity. At the proton energies for which the cross sections are mainly sensitive to the proton widths they are 0.89 ± 0.08, 1.00 ± 0.08, and 1.10 ± 0.09 at c.m. energies of 2.063 MeV, 2.360 MeV, and 2.657 MeV, respectively. As further discussed in the following section, this procedure is confirmed by the fact that also the partial cross sections are reproduced correctly.

Assuming that the modification of the proton widths also applies to the additional transitions appearing in the calculation of the astrophysical reaction rate [Eqs. (1) and (2)], we show the new prediction of the proton capture reactivities in Table II. Those reactivitites are stellar reactivities in contrast to laboratory reactivities. The newly derived coefficients for the REACLIB parametrization [61] are given in Table III. The ratio of the rate calculated with the new parameters to the one obtained from the tables of [50] at different plasma temperatures is shown in Fig. 9. At the relevant temperature of 3 GK, the new rate is higher by 28%. This is well within the expected uncertainty of the previous rate prediction and confirms earlier γ-process calculations [10, 11, 62] and their ^{74}Se abundance.

TABLE II. Stellar reactivity $N_A \langle \sigma v \rangle^*$ and g.s. contribution X (taken from [35]) for ^{74}Ge(p,γ)^{75}As as a function of plasma temperature.

T [GK]	Reactivity [cm^{3}s^{-1}mole^{-1}]	X
0.10	2.564 × 10^{-22}	1.00
0.15	2.264 × 10^{-17}	1.00
0.20	2.733 × 10^{-14}	1.00
0.30	1.912 × 10^{-10}	1.00
0.40	4.908 × 10^{-8}	1.00
0.50	2.479 × 10^{-6}	1.00
0.60	4.848 × 10^{-5}	1.00
0.70	5.137 × 10^{-4}	1.00
0.80	3.560 × 10^{-3}	1.00
0.90	1.809 × 10^{-2}	1.00
1.00	7.272 × 10^{-2}	1.00
1.50	8.946 × 10^{0}	0.95
2.00	1.644 × 10^{2}	0.86
2.50	1.175 × 10^{3}	0.75
3.00	4.738 × 10^{3}	0.66
3.50	1.300 × 10^{4}	0.60
4.00	2.718 × 10^{4}	0.55
4.50	4.674 × 10^{4}	0.51
5.00	6.947 × 10^{4}	0.49
6.00	1.124 × 10^{5}	0.44
7.00	1.357 × 10^{5}	0.40
8.00	1.328 × 10^{5}	0.35
9.00	1.111 × 10^{5}	0.30
10.00	8.357 × 10^{4}	0.24

TABLE III. REACLIB parameters for ^{74}Ge(p,γ) and its reverse reaction, obtained from fitting the reactivities shown in Table II.

Parameter	(p,γ)	(γ,p)
a_0	2.780078×10^1	5.010011×10^1
a_1	0.000000	-8.005979×10^1
a_2	-5.063646×10^1
a_3	2.235434×10^1
a_4	-2.185726
a_5	4.255545×10^{-2}
a_6	-9.282484	-7.782484

TABLE IV. Summary of the experimental partial cross sections listed for each center-of-mass energy $E_{\mathrm{c.m.}}$. For comparison partial cross sections from Ratkevich *et al.* [63] are given as well. Please note the large uncertainties in the energy. This data are marked with asteriks.

$E_{\mathrm{c.m.}}$ [keV]	Energy of level which is directly fed from the "entry state"					
	0 keV $\sigma(\gamma_0)$ [μb]	199 keV $\sigma(\gamma_1)$ [μb]	265 keV $\sigma(\gamma_2)$ [μb]	280 keV $\sigma(\gamma_3)$ [μb]	401 keV $\sigma(\gamma_5)$ [μb]	469 keV $\sigma(\gamma_6)$ [μb]
2063 ± 7	11.8 ± 0.9	9.8 ± 0.7	9.6 ± 1.2	3.2 ± 1.0		7.9 ± 0.6
2360 ± 7	20.8 ± 1.5	19.0 ± 1.4	30.6 ± 2.5	3.8 ± 1.0	7.1 ± 0.7	14.7 ± 1.2
$*2400 \pm 300$	$*22.4 \pm 4.8$	$*19.8 \pm 4.0$	$*19.0 \pm 5.0$	$*3.7 \pm 0.8$	$*7.8 \pm 1.4$	$*15.7 \pm 3.2$
2657 ± 7	41.8 ± 3.1	33.8 ± 2.5	49.5 ± 3.9	12.0 ± 1.3	15.1 ± 1.4	30.3 ± 2.4
2955 ± 7	64.9 ± 4.7	56.8 ± 4.1	73.3 ± 5.6	19.8 ± 2.2	26.1 ± 2.1	44.9 ± 3.4
3251 ± 7	90.0 ± 6.6	62.8 ± 4.8	102.9 ± 7.7	25.4 ± 2.7	39.6 ± 3.7	64.9 ± 5.2
3449 ± 7	82.6 ± 6.1	58.6 ± 4.4	90.5 ± 7.0	26.2 ± 3.0	30.6 ± 2.8	45.1 ± 3.8
3646 ± 8	31.0 ± 2.3	21.7 ± 1.9	32.2 ± 3.2	7.6 ± 1.0	10.3 ± 1.1	19.9 ± 1.7

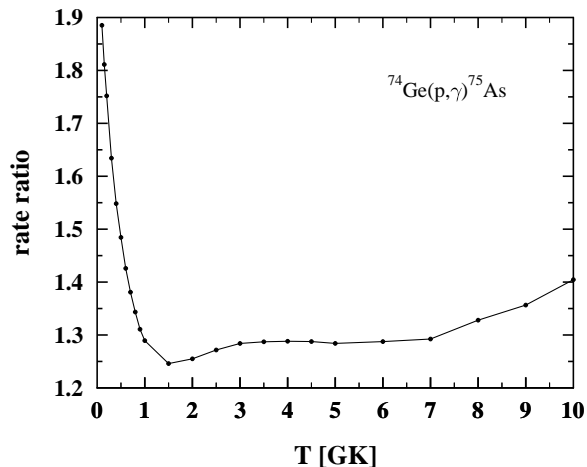| $E_{\mathrm{c.m.}}$ [keV]	Energy of level which is directly fed from the "entry state"					
	572 keV $\sigma(\gamma_7)$ [μb]	618 keV $\sigma(\gamma_8)$ [μb]	865 keV $\sigma(\gamma_{10})$ [μb]	1075 keV $\sigma(\gamma_{12})$ [μb]	1129 keV $\sigma(\gamma_{14})$ [μb]	1204 keV $\sigma(\gamma_{15})$ [μb]
2063 ± 7	2.0 ± 0.3	5.7 ± 0.5	3.1 ± 0.5	8.0 ± 0.7	10.7 ± 0.9	5.4 ± 0.5
2360 ± 7	3.2 ± 0.5	12.4 ± 1.2	9.1 ± 0.9	19.7 ± 1.6	26.5 ± 2.2	13.6 ± 1.3
$*2400 \pm 300$	$*2.7 \pm 1.0$	$*12.8 \pm 2.6$	$*10.8 \pm 3.5$	$*14.1 \pm 3.2$	$*17.5 \pm 1.4$	$*10.2 \pm 2.1$
2657 ± 7	12.2 ± 1.4	25.7 ± 2.3	23.9 ± 2.2	37.2 ± 3.1	39.4 ± 3.2	22.2 ± 2.3
2955 ± 7	16.4 ± 1.7	45.0 ± 3.5	34.5 ± 2.9	57.4 ± 4.4	63.1 ± 4.8	44.0 ± 3.9
3251 ± 7	35.3 ± 3.4	60.9 ± 5.9	54.1 ± 4.7	78.2 ± 6.1	82.7 ± 6.6	51.1 ± 4.5
3449 ± 7	17.9 ± 2.2	45.3 ± 3.8	43.9 ± 3.9	75.0 ± 6.0	87.0 ± 6.9	41.8 ± 3.9
3646 ± 8	9.1 ± 1.4	22.4 ± 2.0	27.4 ± 2.5	31.6 ± 2.9	27.0 ± 2.6	20.6 ± 2.1

FIG. 9. Ratio of the stellar rate from Table II and the rate given in Ref. [50].

B. Partial cross sections

1. Experimental results

In Table IV the measured partial cross sections are shown. Twelve transitions, which feed levels of ^{75}As di-rectly from the entry state, were observed and the partial cross sections for these levels were determined. The transition to the fourth excited state is strongly suppressed because of its spin and parity. The other three missing transitions to the 9th, 11th, and 13th state are visible in the γ spectra, but the low peak-to-background ratio at the respective energies hamper a reliable analysis. Furthermore, a lot of γ-ray transitions to levels with high excitation energy in ^{75}As occur. Because the level scheme of ^{75}As is incomplete in this energy range, those transitions could not be analyzed.

Our results can be compared to values from Ref. [63]. This reference gives a list of partial cross sections for a proton energy of (2.4 ± 0.3) MeV. Please note the large uncertainties for the energy. Their values are included in Table IV. In Ref. [63] the primary γ-ray transitions were measured with a pair spectrometer consisting of a Ge(Li) detector which was surrounded by a four-section circular NaI(Tl) detector. The partial cross sections agree for most transitions with our values within the uncertainties. Nevertheless, there are slightly larger discrepancies for the partial cross sections populating the levels at 265, 1075, and 1129 keV.
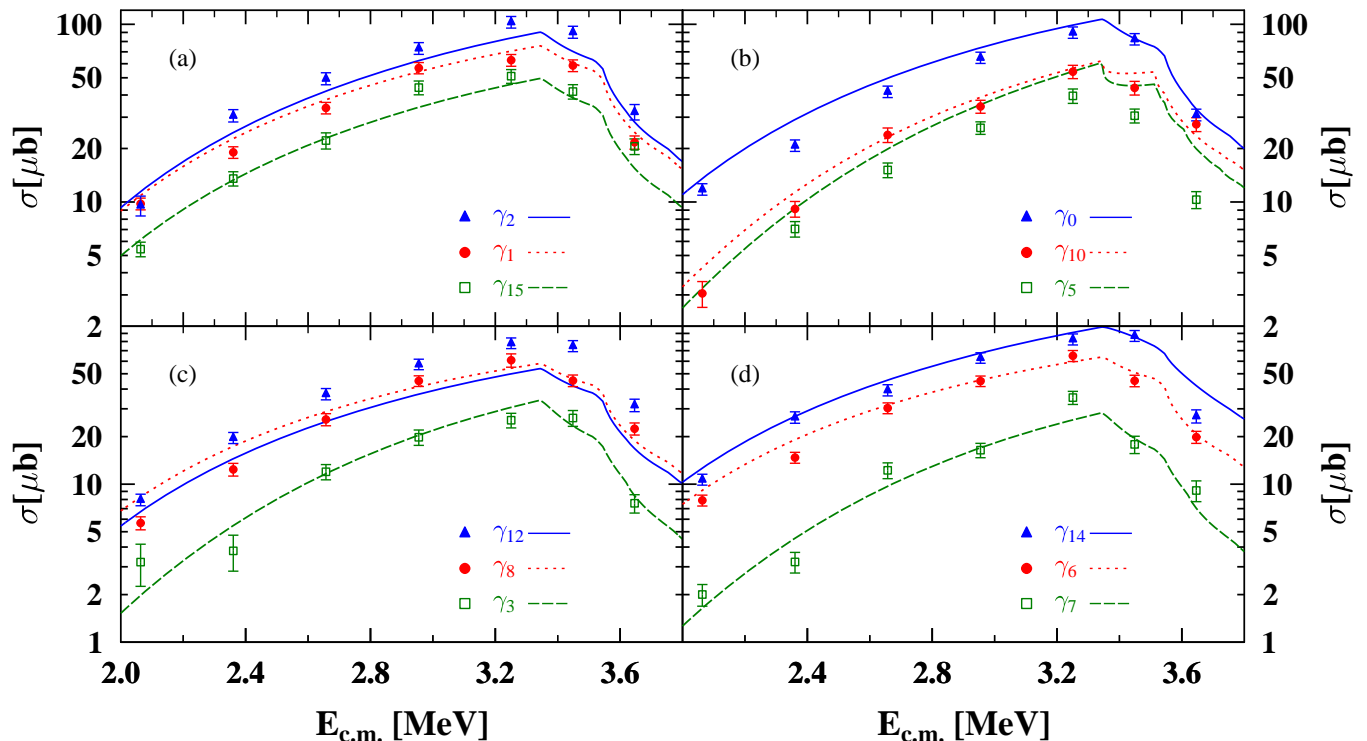
FIG. 10. (Color online) Partial cross sections for the reaction ^{74}Ge(p,γ)^{75}As as a function of center-of-mass energy. Because the symbol widths are larger than the horizontal uncertainties, no horizontal error bars are depicted. The experimental values are compared with predictions calculated with the SMARAGD code using the proton optical model potential of Refs. [51, 52] multiplied by a factor of two.

2. Comparison to theory and new spin assignments to the 401–and 1075–keV states in ^{75}As

The modification of the proton widths obtained with the JLM optical potential discussed in Sec. V A 2 also has to apply to the partial widths. As shown in Fig. 10, the resulting cross section calculation (with the proton widths multiplied by a factor of two) agrees well with the data. There are two exceptions, discrepancies occur for the γ_5 and γ_{12}. These cannot be attributable to a problem in the optical potential as this would systematically affect also the other partial cross sections. Because all other partial cross sections are well reproduced, they have to be explained by incorrect spin or parity assignments.

The prediction of the partial cross sections for the γ_{12} transition from the state at 1075 keV are too low. The spin assignment to this state is $3/2^-$ [42]. We find improved agreement when additionally including a $5/2^-$ state at the same energy, leading to a doublet assignment of "$3/2^-$, $5/2^-$".

The γ_5 case of the partial cross section of the state at 401 keV is different because it is overpredicted by theory. This can only be remedied by changing the parity assignment from $5/2^+$ to $5/2^-$. The original $5/2^+$ assignment quoted in Ref. [42] was obtained from $\ell = 2$ partial waves in DWBA calculations [64–66]. It is conceivable that the data of [64–66] can also be reproduced with $\ell = 3$ but a further DWBA calculation is required for confirmation. It may be noted in passing that the original parity assignment was tentative [67] but was adopted as proven in the subsequent papers, including the Refs. [64–66] cited by Ref. [42].

3. Implications for astrophysical neutron capture on ^{74}As

The sensitivities of the partial cross sections to variations of the different widths are very similar to the ones shown in Fig. 3 for the total cross sections. There is a subtle difference, however, which can be used to extract additional information relevant for astrophysics.

The averaged widths $\langle \Gamma_x \rangle$ of the possible reaction channels $x = \gamma, \mathrm{n}, \mathrm{p}, \alpha$ (i.e., in the γ, neutron, proton, and α channel) enter the calculation of the total (p,γ) cross section in the form of a sum over fractions [34, 35]

$$\sigma \propto \sum_{J,\pi}(2J+1)\frac{\langle \Gamma_\mathrm{p}^0 \rangle \langle \Gamma_\gamma \rangle}{\langle \Gamma_\gamma \rangle + \langle \Gamma_\mathrm{p} \rangle + \langle \Gamma_\mathrm{n} \rangle + \langle \Gamma_\alpha \rangle} \quad , \quad (11)$$

where the superscript on a width indicates a partial width leading to a single final state whereas widths without superscript denote sums of partial widths including all

energetically possible transitions in the given channel,

$$\langle \Gamma_x \rangle = \langle \Gamma_x^0 \rangle + \langle \Gamma_x^1 \rangle + \langle \Gamma_x^2 \rangle + \cdots = \sum_m \langle \Gamma_x^m \rangle \quad . \quad (12)$$

These are transitions connecting the final states m in each channel with a compound (entry) state at a given energy and with spin J and parity π.

The calculation of averaged widths requires certain nuclear properties to be known. For the particle widths these are mainly the level scheme of low-lying levels, as transitions to these dominate the total width [34, 35], and the optical potentials used to compute the strength of each transition. For $\langle \Gamma_\gamma \rangle$, however, these are the photon strength functions determining the strength of each transition and the nuclear level density, as γ-ray transitions to states with high excitation energy dominate, above the region of well resolved, isolated levels [68]. A variation of any of these properties translates into a variation of the width and the sensitivities s shown in Figs. 2 and 3 make it possible to judge the impact on the rate and cross section.

Equation (11) holds for the total cross section, whereas for the partial cross sections a slightly modified version applies,

$$\sigma^m \propto \sum_{J,\pi}(2J+1)\frac{\langle \Gamma_p^0 \rangle \langle \Gamma_\gamma^m \rangle}{\langle \Gamma_\gamma \rangle + \langle \Gamma_p \rangle + \langle \Gamma_n \rangle + \langle \Gamma_\alpha \rangle} \quad . \quad (13)$$

The only difference is found in the numerator where the total γ width is replaced by the partial width leading to state m. This explains the different behavior of the partial cross sections to a variation of the nuclear level density in ^{75}As. A variation of the nuclear level density only affects the total width $\langle \Gamma_\gamma \rangle$ which sums (or integrates) over all accessible levels, as shown in Eq. (12), whereas obviously it does not enter the partial width $\langle \Gamma_\gamma^m \rangle$. Because the total γ width appears both in the numerator and denominator of Eq. (11), the sensitivity to a variation of the nuclear level density is the same as to a multiplication of the γ width with a factor. For the energy range interesting for the γ process we found no sensitivity to such a variation, as illustrated by Fig. 3.

However, Fig. 11 shows the sensitivity of the cross section for ^{74}Ge(p,γ_0)^{75}As as an example for the sensitivities of partial cross sections to a variation of the nuclear level density in ^{75}As. A nonzero sensitivity is found also below the (p,n) threshold, in the astrophysically relevant energy range. The negative values shown imply that the cross section changes opposite to the variation factor of the nuclear level density; that is, the cross section decreases when the level density is increased and vice versa. This can easily be understood by realizing that the total γ width, which is modified by a change in the level density, is appearing only in the denominator of the width ratio in Eq. (13). If $\langle \Gamma_\gamma \rangle$ comprises a large part of the denominator (and this is the case as the α and proton widths are very small and we are below the neutron emission
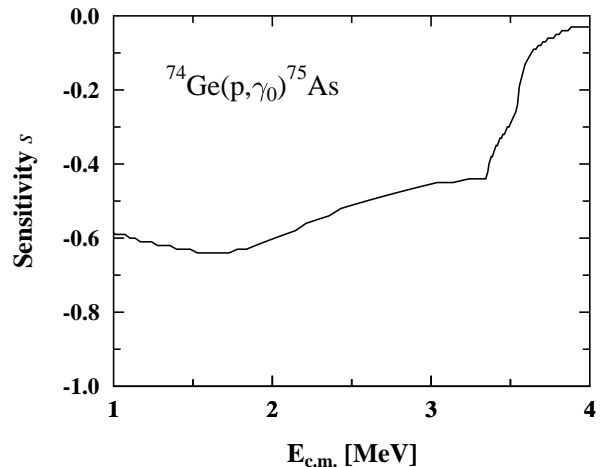

FIG. 11. Sensitivity s of the ^{74}Ge(p,γ_0)^{75}As partial cross section when varying the nuclear level density in the γ channel by a factor of two. Negative sensitivities imply that the cross section is changed opposite to the variation of the level density.

threshold), the variation cannot cancel with the numerator, as it would be the case for the total cross section. It is important to note, however, that a multiplication of both the partial and total γ width by the same factor would again lead to the same sensitivity as given by Eq. (11) and shown in Fig. 3. This would be equivalent to a (energy-independent) variation of the photon strength function.

Total *and* partial cross sections, and their energy dependence, are well reproduced by theory when using modified proton widths across the measured energy range. Because the sensitivities of the partial cross section to the γ widths change with energy, this leads to the conclusion that the γ widths are predicted well without need of further modification. This includes the combination of photon strength function and nuclear level density in ^{75}As entering the γ width in the total cross sections as well as the nuclear level density of ^{75}As at the excitation energies relevant for the γ-ray transitions.

It was shown that the relevant excitation energies of the final states of the γ-ray transitions dominating $\langle \Gamma_\gamma \rangle$ are located $2 - 4$ MeV below the compound formation energy [68]. It is a curious fact that these relevant energies are very similar for the reactions ^{74}Ge(p,γ)^{75}As and ^{74}As(n,γ)^{75}As at the same astrophysical plasma temperature [38]. Hence, these two reactions, which have the same exit channel, can be described with the same γ widths. In addition, the ^{74}As(n,γ) rate at γ process temperatures is exclusively sensitive to the γ widths [35]. As a consequence the ^{74}As(n,γ) rate is predicted well using the standard γ widths of the current version of the SMARAGD code.

As for the ^{74}Ge(p,γ)^{75}As reaction, we also give the

TABLE V. Stellar reactivity $N_A \langle \sigma v \rangle^*$ and g.s. contribution X (taken from [35]) for ^{74}As$(n,\gamma)^{75}$As as function of plasma temperature.

T [GK]	Reactivity [cm^{3}s^{-1}mole^{-1}]		X
		$\times$	
0.10	1.035	$\times$ 10^8	1.00
0.15	1.058	$\times$ 10^8	1.00
0.20	1.088	$\times$ 10^8	1.00
0.30	1.145	$\times$ 10^8	1.00
0.40	1.185	$\times$ 10^8	0.99
0.50	1.198	$\times$ 10^8	0.97
0.60	1.180	$\times$ 10^8	0.93
0.70	1.136	$\times$ 10^8	0.89
0.80	1.076	$\times$ 10^8	0.83
0.90	1.008	$\times$ 10^8	0.78
1.00	9.414	$\times$ 10^7	0.72
1.50	6.853	$\times$ 10^7	0.50
2.00	5.423	$\times$ 10^7	0.36
2.50	4.555	$\times$ 10^7	0.27
3.00	3.965	$\times$ 10^7	0.21
3.50	3.523	$\times$ 10^7	0.17
4.00	3.165	$\times$ 10^7	0.14
4.50	2.855	$\times$ 10^7	0.11
5.00	2.573	$\times$ 10^7	0.10
6.00	2.054	$\times$ 10^7	0.07
7.00	1.581	$\times$ 10^7	0.05
8.00	1.165	$\times$ 10^7	0.04
9.00	8.247	$\times$ 10^6	0.03
10.00	5.650	$\times$ 10^6	0.02

TABLE VI. REACLIB parameters for ^{74}As(n,γ) and its reverse reaction, obtained from fitting the reactivities shown in Table V.

Parameter	(n,γ)	(γ,n)
a_0	6.592306×10^1	8.983183×10^1
a_1	-4.470440×10^{-1}	-1.193209×10^2
a_2	3.601952×10^1	
a_3	-8.985803×10^1	
a_4	7.297599	
a_5	-5.682330×10^{-1}	
a_6	3.457422×10^1	3.607422×10^1

reactivities and REACLIB fit coefficients for the reaction ^{74}As$(n,\gamma)^{75}$As in Tables V and VI, and show a comparison to the rate from Ref. [50] in Fig. 12. The new rate differs only by a few percent from the rate given in Ref. [50] but the information gained from the present (p,γ) measurement puts the rate on a firmer basis.

In the astrophysical γ process, the ^{75}As$(\gamma,n)^{74}$As rate competes with the ^{75}As(γ,p) and ^{75}As(p,n) rates and therefore also impacts the production of ^{74}Se. Moreover, when this reaction is well predicted it is also likely that the reaction rate for ^{75}Se$(\gamma,n)^{74}$Se is predicted equally well.
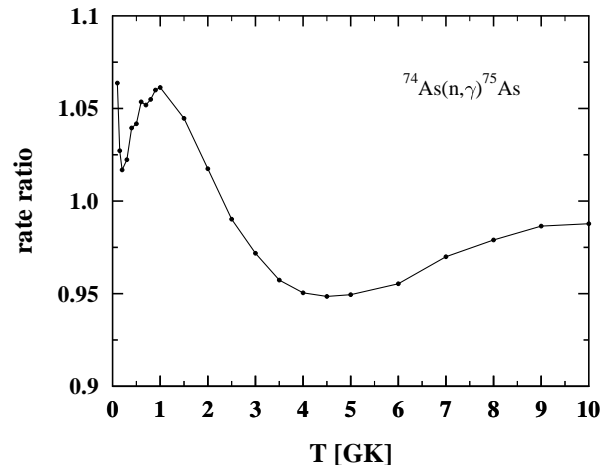

FIG. 12. Ratio of the stellar rate from Table V and the rate given in Ref. [50].

VI. SUMMARY AND CONCLUSION

The total cross sections of the reaction ^{74}Ge$(p,\gamma)^{75}$As were measured between 2.1 MeV and 3.7 MeV using the in-beam γ spectroscopy technique with HPGe detectors of high efficiency. This energy range covers a considerable fraction of the astrophysically relevant energy range and thus the results make it possible to draw conclusions for the prediction of the astrophysical reaction rate used in γ-process simulations. The in-beam technique with high-resolution detectors is a very sensitive tool that allows, in addition to the determination of total cross sections, the investigation of partial cross sections as well. Twelve of the direct feeding transitions were observed and investigated.

The astrophysical conclusions drawn are important for the synthesis of the lightest p nuclide, ^{74}Se. Using the present data, it was possible to improve the predictions of cross sections and also of the astrophysical reaction rate for ^{74}Ge$(p,\gamma)^{75}$As (and its reverse reaction). A renormalization of the proton width of the ^{74}Ge(p,γ) reaction by a factor of two was required to achieve a good reproduction of the magnitude of the total cross sections and their energy dependence. The same renormalization can consistently reproduce the partial cross sections of this reaction. This factor of two is probably attributable to deficiencies in the p+^{74}Ge optical potential, which calls for further investigations and will be important to improve the global optical potential. Nevertheless, the derived astrophysical reaction rate is higher by only about 28% than the previous prediction by Ref. [50].

The combination of partial and total cross sections allowed further conclusions which were specific for this case. The combined data allowed to test the prediction of the ^{74}As$(n,\gamma)^{75}$As cross sections at the astrophysically relevant energies. This allowed to put the prediction of

this reaction (and its reverse) on a firm grounding. The newly calculated rate, however, differs only by a few percent from the rate standard given in Ref. [50].

Finally, our calculations were sensitive enough to check the spin and parity assignments of the excited states appearing as final states in the partial cross sections. To describe the data, it was necessary to use a $3/2^-$, $5/2^-$ doublet at 1075 keV, contrary to the $3/2^-$ assignment in Ref. [42]. A change in parity from $5/2^+$ to $5/2^-$ was required for the final state at 401 keV.

The above results underline the power of the in-beam technique with high-efficiency detectors, combined with a sensitivity analysis of the cross sections, as a tool for nuclear astrophysics as well as nuclear structure investigations.

ACKNOWLEDGMENTS

[1] C. Arlandini, F. Käppeler, K. Wisshak, R. Gallino, M. Lugaro, M. Busso, and O. Straniero, Astrophys. J. **525**, 886 (1999).

[2] Zs. Nemeth, F. Käppeler, C. Theis, T. Belgya, and S. W. Yates, Astrophys. J. **426**, 357 (1994).

[3] M. Arnould and S. Goriely, Phys. Rep. **384**, 1 (2003).

[4] E. M. Burbidge, G. R. Burbidge, W. A. Fowler, and F. Hoyle, Rev. Mod. Phys. **29**, 547 (1957).

[5] A. G. W. Cameron, Pub. Astron. Soc. Pac. **69**, 201 (1957).

[6] J. J. Cowan, F.-K. Thielemann, and J. W. Truman, Phys. Rep. **208**, 267 (1991).

[7] F. Käppeler, R. Gallino, S. Bisterzo, and W. Aoki, Rev. Mod. Phys. **83**, 157 (2011).

[8] M. Arnould, S. Goriely, and K. Takahashi, Phys. Rep. **450**, 97 (2007).

[9] M. Rayet, M. Arnould, M. Hashimoto, N. Prantzos, and K. Nomoto, Astron. Astrophys. **298**, 517 (1995).

[10] T. Rauscher, A. Heger, R. D. Hoffman, and S. E. Woosley, Astrophys. J. **576**, 323 (2002).

[11] S. E. Woosley and A. Heger, Phys. Rep. **442**, 269 (2007).

[12] S. E. Woosley and W. M. Howard, Astrophys. J. Suppl. **36**, 285 (1978).

[13] T. Rauscher, PoS(NIC XI)059 (2010).

[14] H. Schatz, A. Aprahamian, J. Görres, M. Wiescher, T. Rauscher, J. F. Rembges, F.-K. Thielemann, B. Pfeiffer, P. Möller, K.-L. Kratz, H. Herndl, B. A. Brown, and H. Rebel, Phys. Rep. **294**, 167 (1998).

[15] H. Schatz, A. Aprahamian, V. Barnard, L. Bildsten, A. Cumming, M. Ouellette, T. Rauscher, F.-K. Thielemann, and M. Wiescher, Phys. Rev. Lett. **86**, 3471 (2001).

[16] S. Goriely, J. Jose, M. Hernanz, M. Rayet, and M. Arnould, Astron. Astrophys. **383**, L27 (2002).

[17] C. Fröhlich, G. Martínez-Pinedo, M. Liebendörfer, F.-K. Thielemann, E. Bravo, W. R. Hix, K. Langanke, and N. T. Zinner, Phys. Rev. Lett. **96**, 142502 (2006).

[18] S. E. Woosley, D. H. Hartmann, R. D. Hoffman, and W. C. Haxton, Astrophys. J. **356**, 272 (1990).

[19] C. Travaglio, F. K. Röpke, R. Gallino, and W. Hillebrandt, Astrophys. J. **739**, 93 (2011).

[20] W. M. Howard, B. S. Meyer, and S. E. Woosley, Astrophys. J. Lett. **373**, L5 (1991).

[21] W. M. Howard and B. S. Meyer, in *Proceedings of 2nd International Conference Nuclei in the Cosmos*, edited by F. Käppeler and K. Wisshak (IOP Publishing, Bristol 1993), p. 575.

[22] M. Kusakabe, N. Iwamoto, and K. Nomoto, Nucl. Phys. **A758**, 459 (2005).

[23] W. Hauser and H. Feshbach, Phys. Rev. **87**, 366 (1952).

[24] W. Rapp, J. Görres, M. Wiescher, H. Schatz, and F. Käppeler, Astrophys. J. **653**, 474 (2006).

[25] T. Rauscher, Phys. Rev. C **73**, 015804 (2006).

[26] S. Harissopulos, E. Skreti, P. Tsagari, G. Souliotis, P. Demetriou, T. Paradellis, J. W. Hammer, R. Kunz, C. Angulo, S. Goriely, and T. Rauscher, Phys. Rev. C **64**, 055804 (2001).

[27] S. Galanopoulos, P. Demetriou, M. Kokkoris, S. Harissopulos, R. Kunz, M. Fey, J. W. Hammer, Gy. Gyürky, Zs. Fülöp, E. Somorjai, and S. Goriely, Phys. Rev. C **67**, 015801 (2003).

[28] C. Yalçin, R. T. Güray, N. Özkan, S. Kutlu, Gy. Gyürky, J. Farkas, G. G. Kiss, Zs. Fülöp, A. Simon, E. Somorjai, and T. Rauscher , Phys. Rev. C **79**, 065801 (2009).

[29] D. Filipescu, V. Avrigeanu, T. Glodariu, C. Mihai, D. Bucurescu, M. Ivasşcu, I. Căta-Danil, L. Stroe, O. Sima, G. Căta-Danil, D. Deleanu, D. G. Ghiţă, N. Mărginean, A. Negret, S. Pascu, T. Sava, G. Suliman, and N. V. Zamfir, Phys. Rev. C **83**, 064609 (2011).

[30] I. Dillmann, L. Coquard, C. Domingo-Pardo, F. Käppeler, J. Marganiec, E. Uberseder, U. Giesen, A. Heiske, G. Feinberg, D. Hentschel, S. Hilpp, H. Leiste, T. Rauscher, and F.-K. Thielemann, Phys. Rev. C **84**, 015802 (2011).

[31] G. G. Kiss, T. Rauscher, T. Szücs, Zs. Kertész, Zs. Fülöp, Gy. Gyürky, C. Fröhlich, J. Farkas, Z. Elekes, and E. Somorjai, Phys. Lett. B **695**, 419 (2011).

[32] Z. Halász, Gy. Gyürky, J. Farkas, Zs. Fülöp, T. Szücs, E. Sormorjai, and T. Rauscher, Phys. Rev. C **85** 025804 (2012).

[33] A. Sauerwein, H.-W. Becker, H. Dombrowski, M. Elvers, J. Endres, U. Giesen, J. Hasper, A. Hennig, L. Netterdon, T. Rauscher, D. Rogalla, K. O. Zell, and A. Zilges, Phys. Rev. C **84** 045808 (2011).

[34] T. Rauscher, Int. J. Mod. Phys. E **20**, 1071 (2011).

[35] T. Rauscher, Astrophys. J. Suppl., **201**, 26 (2012).

[36] W. A. Fowler, Quart. J. Roy. Astron. Soc. **15**, 82 (1974).

[37] T. Rauscher, P. Mohr, I. Dillmann, and R. Plag, Astrophys. J. **738**, 143 (2011).

[38] T. Rauscher, Phys. Rev. C **81**, 045807 (2010).

[39] NNDC Online Data Service, Q-value Calculator, http://www.nndc.bnl.gov/qcalc/ .

[40] J. F. Ziegler and J. P. Biersack, Code SRIM, Version 2008.04. Full description given by J. F. Ziegler, J. P. Biersack, and U. Littmark, *The Stopping and Range of Ions in Solids* (Pergamon, New York, 1985).

[41] S. Agostinelli *et al.*, Nucl. Instr. and Meth. A **506**, 250 (2003).

[42] Evaluated Nuclear Structure Datafile (ENSDF) 2012, online database at `http://www.nndc.bnl.gov/ensdf/`, retrieved May 16, 2012.

[43] A. Anttila, J. Keinonen, M. Hautala, and I. Forsblom, NIM **147** 501 (1977).

[44] P. M. Endt, C. Alderliesten, F. Zijderhand, A. A. Wolters, and A. G. M. Van Hees, Nucl. Phys. **A510**, 209 (1990).

[45] C. E. Rolfs and W. S. Rodney, *Claudrons in the Cosmos* (The University of Chicago Press, Chicago, 1988).

[46] C. E. Rolfs, Nucl. Phys. News, **16(2)**, 9 (2006).

[47] K. U. Kettner, H.-W. Becker, F. Schrieder, and C. Rolfs, J. Phys. G: Nucl. Part. Phys. 32, 489 (2006).

[48] A. Spyrou, A. Lagoyannis, P. Demetriou, S. Harissopulos, and H.-W. Becker, Phys. Rev. C **77**, 065801 (2008).

[49] T. Rauscher, code SMARAGD, version 0.8.4s (2012).

[50] T. Rauscher and F.-K. Thielemann, At. Data Nucl. Data Tables **79**, 47 (2001).

[51] J.-P. Jeukenne, A. Lejeune, and C. Mahaux, Phys. Rev. C **15**, 10 (1977).

[52] A. Lejeune, Phys. Rev. C **21**, 1107 (1980).

[53] M. Samyn, S. Goriely, P.-H. Heenen, J. M. Pearson, and F. Tondeur, Nucl. Phys. **A700**, 142 (2002).

[54] S. Goriely, M. Samyn, and J. M. Pearson, Phys. Rev. C **75**, 064312 (2007).

[55] J. W. Negele, Phys. Rev. C **1**, 1260 (1970).

[56] G. G. Kiss, Gy. Gyürky, Z. Elekes, Zs. Fülöp, E. Somorjai, T. Rauscher, and M. Wiescher, Phys. Rev. C **76**, 055807 (2007).

[57] G. G. Kiss, T. Rauscher, Gy. Gyürky, A. Simon, Zs. Fülöp, and E. Somorjai, Phys. Rev. Lett. **101**, 191101 (2008).

[58] T. Rauscher, G. G. Kiss, Gy. Gyürky, A. Simon, Zs. Fülöp, E. Somorjai, Phys. Rev. C 80 (2009) 035801.

[59] E. Bauge, J. P. Delaroche, and M. Girod, Phys. Rev. C **58**, 1118 (1998).

[60] E. Bauge, J. P. Delaroche, and M. Girod, Phys. Rev. C **63**, 024607 (2001).

[61] T. Rauscher and F.-K. Thielemann, At. Data Nucl. Data Tables **75**, 1 (2000).

[62] I. Dillmann, T. Rauscher, M. Heil, F. Käppeler, W. Rapp, and F.-K. Thielemann, J. Phys. G **35**, 014029 (2008).

[63] S. S. Ratkevich, B. A. Nemashkalo, and I. D. Fedorets, Phys. Atomic Nuclei **60**, 713 (1997), translated from Yad. Fiz. **60**, 804 (1997).

[64] R. R. Betts, S. Mordechai, D. J. Pullen, B. Rosner, and W. Scholz, Nucl. Phys. **A230**, 235 (1974).

[65] M. Schrader, H. Reiss, G. Rosner, and H. V. Klapdor, Nucl. Phys. **A263**, 193 (1976).

[66] G. Rotbard, M. Vernes, J. Vernotte, G. Berrier-Rosin, J. Kalifa, R. Tamisier, Nucl. Phys. **A401** 41 (1983).

[67] S. C. Pancholi and H. Ikegami, Nucl. Data Sheets B **1**, 79 (1966).

[68] T. Rauscher, Phys. Rev. C **78**, 032801(R) (2008).